Role of Bond on Crack Width in Reinforced Concrete Members in Tension

P. Bernardi, R. Cerioni, D. Ferretti* and E. Michelini

Department of Civil and Environmental Engineering and Architecture,
University of Parma
P.co Area delle Scienze 181/A, 43124 PARMA, ITALY
Fax: +39-(0)521-905924, *e-mail: daniele.ferretti@unipr.it

ABSTRACT. *This paper aims to investigate the effectiveness of 1D numerical models in representing the global and local behaviour of reinforced concrete tension ties. These simplified approaches, mainly based on bond, neglect the contribution of stress diffusion in concrete blocks between cracks, which has been recognised as one of the most influencing parameters, especially for the evaluation of crack width. To investigate the influence of this assumption, a simplified 1D model has been here developed and verified through comparisons with reliable experimental data, as well as with results provided by a more refined 2D Finite Element model. The main results have shown that simplified models appear to be suitable to investigate local behaviour of the analysed elements and can be adopted to perform extensive parametric studies investigating the main variables influencing crack width.*

INTRODUCTION

The presence of cracks in reinforced concrete (RC) structures influences many aspects of their behaviour, particularly concerning serviceability, durability, aesthetics and force transfer [1]. Several experimental and theoretical studies have been directed to the determination of crack width and spacing, pointing out the most influencing parameters and providing relationships for their determination. Anyway, the problem of the evaluation of crack width is still open. In order to understand the involved mechanisms, researchers preferred to analyse tension ties, which can be studied easier than beams and whose results can be extended to any other tension zone.

One of the difficulties encountered in the calibration of crack formulae arises from the statistical dispersion of experimental data, both regarding material properties (particularly concrete tensile strength), and the measured quantities (maximum or average crack widths, initial or stabilised crack spacing). Moreover, crack widths can be measured at surface, at bar level or at midway, and the type of adopted instrumentation (microscope or extensometer) has a relevant influence too. From experimental and numerical studies, two main phenomena have been recognised as the most important: diffusion of stresses in concrete blocks delimited by cracks [2, 3], and bond between reinforcing steel and concrete [4]. Recently, Beeby [5, 6] has questioned the role of bond on crack width, which seems to be overshadowed by diffusion of stresses. In [5]

the critical variable defining cracking behaviour has been indeed recognised in the concrete cover rather than in the bond parameters, which are however assumed as fundamental in the classical theory of cracking. Concrete cover also influences the crack shape, since crack width at the concrete surface is wider than at bar surface [7]. For these reasons, in order to completely understand the stress transfer mechanisms of a tension tie, proper 3D or 2D numerical models should be adopted so to consider an effective local bond-slip law and the diffusion of stresses. Anyway, for simplicity, the problem is usually studied in one dimension, that is along the tension tie axis, by describing the behaviour with equilibrium and compatibility equations [8], neglecting stress diffusion. In this paper a numerical 1D model has been developed to study the effect of bond on crack width. The model has been validated with experimental data and then its effectiveness in reproducing the physical reality has been also discussed by comparing the obtained results with those of a more refined 2D Finite Element model.

PROPOSED 1D NUMERICAL MODEL FOR TENSION TIES

For the analysis of a RC tension tie, i.e. a steel bar surrounded by a concrete prism (Fig. 1a), a numerical model based on bond between steel and concrete has been developed. The model has been derived from a previous work [9] on RC tensile members strengthened by FRP plates, by removing the FRP contribution.

Kinematics, equilibrium and compatibility equations

The transverse cross-section of the concrete prism is assumed to remain plane after deformation. Hence, with reference to Fig. 1b, concrete and steel bars are subjected to uniform axial strains, denoted by ε_c and ε_s respectively, and the slip s at concrete-steel interface is defined as the relative displacement $s = u_s - u_c$ of two points belonging to steel and concrete that were initially in contact. The slip s is associated to a shear stress τ at the interface (Fig. 1a), which is ruled by a suitable local bond-slip relationship $\tau(s) = k_s(s)\, s$, being k_s a secant stiffness. Bond produces a variation of forces in steel and concrete. Considering the free body diagram of an element of infinitesimal length, equilibrium and compatibility equations for concrete and steel bar are:

$$\begin{aligned}
&\frac{\mathrm{d}N_s(x)}{\mathrm{d}x} = n_b\ \pi\ \phi\ \tau(s) = n_b\ \pi\ \phi\ k_s\left(u_s(x) - u_c(x)\right) \\
&\frac{\mathrm{d}N_c(x)}{\mathrm{d}x} = -n_b\ \pi\ \phi\ \tau(s) = -n_b\ \pi\ \phi\ k_s\left(u_s(x) - u_c(x)\right) \\
&\frac{\mathrm{d}u_s(x)}{\mathrm{d}x} = \varepsilon_s(x) = \frac{N_s(x)}{E_s\ A_s}\ ;\ \ \frac{\mathrm{d}u_c(x)}{\mathrm{d}x} = \varepsilon_c(x) = \frac{N_c(x)}{E_c\ A_c}
\end{aligned} \tag{1}$$

where n_b and ϕ are the number and diameter of steel bars, A_s, A_c and E_s, E_c are the areas and the Young modulus of steel and concrete, respectively.

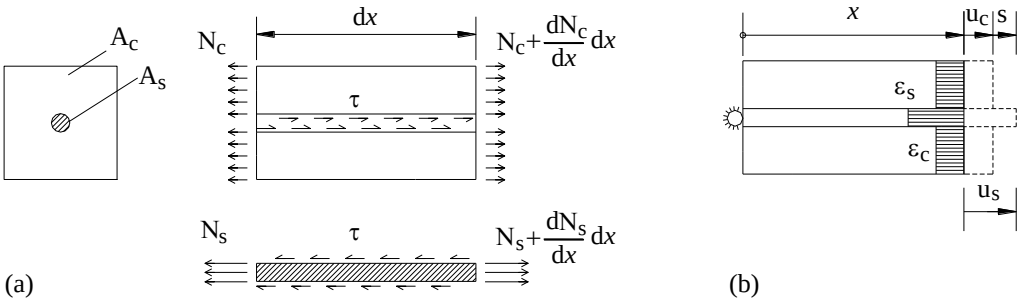

Figure 1. Basic assumptions on (a) equilibrium conditions and (b) kinematics.

Constitutive and interface laws

Reinforcing bars are considered to be linear elastic, as well as linear elastic is the behaviour of concrete in tension until the reaching of its tensile strength f_{ct}. When this is attained, a transversal crack appears and the fictitious crack model is used to define the cohesive tensile stresses σ_{ct} as a function of the fictitious crack opening w. Furthermore, as highlighted in several displacement-controlled tests, when a new transversal crack appears and grows, a partial closure of previously formed cracks occurs. Therefore, both loading and unloading curves are defined, following the cyclic model proposed by Hordijk [10], Fig. 2a.

Bond behaviour between reinforcing steel and concrete is modelled by applying the classical monotonic bond-slip relationship proposed in MC2010 ([11], Fig. 2b). A scaled-down bond strength due to reduced boundary restraints close to the free surfaces (i.e. member ends and transversal cracks) is also considered according to [11]. More in details, bond stresses are reduced by a factor $\lambda = 0.5\ x / \phi \leq 1$ for those parts of the reinforcement at a distance $x \leq 2\phi$ from a transverse crack. Also in this case a cyclic behaviour is introduced (Fig. 2b), since the appearance of a new crack and the consequent reduction of axial load causes unloading at steel-concrete interface, with slips that in some cases may even reverse their sign [9]. Anyway, the damage caused on bond strength (evaluated accordingly to [11]) can be neglected, since the cyclic behaviour seems to be not so significant, due to the small values of residual slips and, consequently, of dissipated energy.

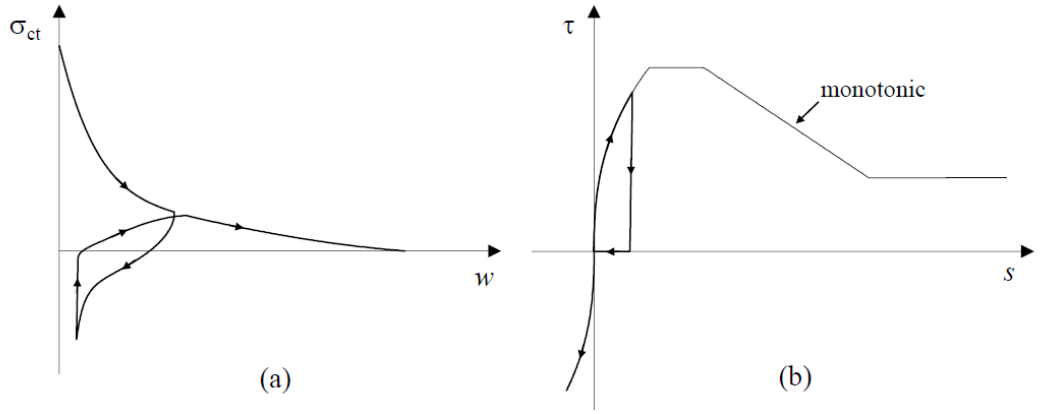

Figure 2. Constitutive laws: (a) concrete in tension [10], (b) bond-slip model [11].

Numerical solution through Finite Difference Method (FDM)

The system of differential equations that governs the problem (Eq. 1) can be rewritten in compact form as:

$$\mathbf{y}'(x) = \mathbf{A}(\mathbf{y}, x)\ \mathbf{y}(x) \qquad 0 \le x \le L \tag{2}$$

where $\mathbf{y}(x) = \{N_s(x)\ \ N_c(x)\ \ u_s(x)\ \ u_c(x)\}^T$ is the vector collecting the unknown functions.

Boundary conditions at the two ends $x = 0,\ L$ of the member, represented in Fig. 3 for both displacement and load control, can be written as:

$$\mathbf{B}_a\ \mathbf{y}(0) + \mathbf{B}_b\ \mathbf{y}(L) = \mathbf{a}\,, \tag{3}$$

where vector **a** takes different forms if the axial force P or, alternatively, the axial elongation ΔL is prescribed. The extended form for matrices $\mathbf{A}(\mathbf{y},x)$, $\mathbf{B}_a$, $\mathbf{B}_b$ and vector **a** are reported in Appendix A.

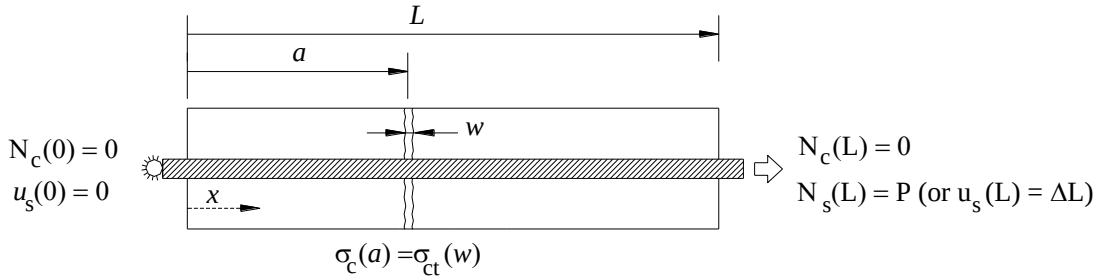

Figure 3. Boundary conditions at the ends of the tensile member.

Eqs. 2 and 3 represent a non-linear boundary value problem that is solved herein through FDM. Following the algorithm proposed in [12], the interval $[0, L]$ is divided using N nodes at uniform distance h, i.e. $0 = x_0 < x_1 < \cdots < x_N = L$. For the j-th node ($0 < j < N$), the derivative in Eq. 2 is replaced by its finite difference approximation $\mathbf{y}'_{j+1/2} \approx (\mathbf{y}_{j+1} - \mathbf{y}_j) / h$ centred at $x_{j+1/2}$. Finite difference equations, together with boundary conditions (Eq. 3), lead to the following non-linear system:

$$\begin{bmatrix} \mathbf{S}_1 & \mathbf{R}_1 & & & & & \\ & \mathbf{S}_2 & \mathbf{R}_2 & & & & \\ & & \ddots & \ddots & & & \\ & & & \mathbf{S}_j & \mathbf{R}_j & & \\ & & & & \ddots & \ddots & \\ & & & & & \mathbf{S}_N & \mathbf{R}_N \\ \mathbf{B}_a & & & & & & \mathbf{B}_b \end{bmatrix} \begin{Bmatrix} \mathbf{y}_0 \\ \mathbf{y}_1 \\ \vdots \\ \mathbf{y}_j \\ \vdots \\ \mathbf{y}_{N-1} \\ \mathbf{y}_N \end{Bmatrix} = \begin{Bmatrix} \mathbf{0} \\ \mathbf{0} \\ \vdots \\ \mathbf{0} \\ \vdots \\ \mathbf{0} \\ \mathbf{a} \end{Bmatrix} \tag{4}$$

where $\mathbf{S}_j = -\mathbf{I} / h - \mathbf{A}((\mathbf{y}_j+\mathbf{y}_{j+1})/2,\ x_{j+1/2}) / 2$, $\mathbf{R}_j = +\mathbf{I} / h - \mathbf{A}((\mathbf{y}_j+\mathbf{y}_{j+1})/2,\ x_{j+1/2}) / 2$ and $\mathbf{I}$ is the identity matrix. To solve the system, the external action P or ΔL is applied in steps. For the generic step, the solution is obtained iteratively updating the secant stiffnesses in Eq. 4 and using as initial guess the solution found at the previous step.

When the tensile stress in concrete reaches the strength f_{ct} in the j-th node, a transversal crack is introduced in concrete by replacing the j-th row of system (Eq. 4) by the internal boundary conditions $\mathbf{B}_c \mathbf{y}_j + \mathbf{B}_d \mathbf{y}_{j+1} = \mathbf{b}$ (w_j), where the crack width $w_j = u_{c,j+1} - u_{c,j}$. Matrices $\mathbf{B}_c$ and $\mathbf{B}_d$ are reported in extended form in Appendix A.

MODEL VALIDATION

The effectiveness of the proposed procedure has been verified through comparisons with significant experimental results on tension ties presented by Wu & Gilbert [13, 14]. The attention has been focused on two specimens, named STN12 and STN16, whose geometrical details are represented in Fig. 4. For concrete and steel mechanical properties, the values reported in [14] have been adopted, that is f_{ct} = 2.0 MPa, f_c = 21.6 MPa, E_c = 22400 MPa, f_{sy} = 540 MPa and E_s = 200000 MPa. The considered experimental tests were carried out under displacement control, by applying a monotonically increasing axial deformation at the ends of the steel bar. As the applied load increased, the evolution of some variables (i.e. the development of crack pattern, the specimen elongation and the steel strains) has been experimentally monitored, so allowing some interesting comparisons with the results obtained from numerical analyses. These latter have been performed by considering the proposed 1D model implemented into a Matlab routine, as well as a 2D FE model (Fig. 4) taking into account both bond effects and stress diffusion in concrete, so to compare their effectiveness in representing the global and local behaviour of the considered ties.

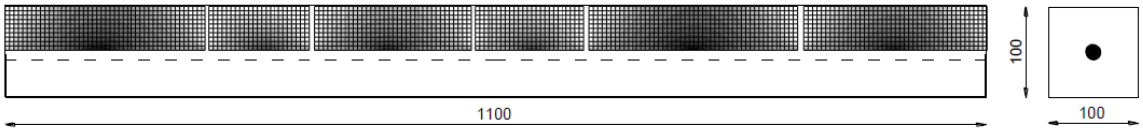

STN12: ϕ= 12 mm; STN16 :ϕ= 16 mm

Figure 4. Dimensions (in mm) of the considered tension ties [14], FE mesh and qualitative axial stress distribution in concrete blocks limited by cracks.

2D Finite Element Modelling

As regards 2D finite element analyses, taking advantage of the symmetry of the problem, only one half of each tie has been modelled, by placing the axis of symmetry at mid-height of the transversal cross-section, along the steel bar axis (Fig. 4). Two-node linear beam elements have been used for reinforcing bar, while four-node plane stress membrane elements with full integration have been adopted for the surrounding concrete (Fig. 4). The corresponding nodes, respectively belonging to concrete and steel, have been linked together by adopting 2D connector elements, called "translators", available in the adopted FE code library (ABAQUS, [15]). These provide a slot connection between the nodes and align their three local axis directions, so allowing for a finite slip between them. To this scope, an elastic-plastic behaviour, properly calibrated on the basis of the adopted MC2010 bond-slip law, has been

assigned to these elements, while a linear elastic behaviour has been adopted both for concrete and reinforcing steel elements. The presence of cracks has been taken into account by using a discrete approach, which consists in generating double coincident nodes along some predefined cracked sections, whose position is known from experimental results. At the beginning of the analysis, these double nodes have been linked together through rigid beam connector elements, which enforce them to have the same displacements, so to model tension tie behaviour in the uncracked stage. As load increases, these connections have been progressively removed on each cracked section, so to simulate the experimental crack formation (Fig. 4). Numerical analyses have been performed under loading control, by applying a monotonically increasing axial load to the external nodes of the reinforcing bar.

Comparisons between numerical simulations and experimental results

To better compare the results provided by the two numerical approaches, simplified 1D analyses have been also carried out by neglecting both the cohesion at crack surfaces and the reduction in bond strength near free surfaces. Moreover, the position of cracks and the cracking loads have been forced to be coincident with the experimental evidences, even if a quite similar crack pattern could be also obtained automatically through the proposed FD procedure.

A first comparison has been performed in terms of axial load-average strain response, as reported in Fig. 5. As can be seen, both the simplified 1D model and the 2D FE simulation provide a quite similar response, which fits quite well the experimental behaviour, both in the first cracking stage and in the last branch of the curve, where a reduction of tension stiffening contribution due to bond deterioration can be observed as the loading increases. At this last stage, the experimental response tends indeed to that of the bare bar, probably due to an extensive micro-cracking near the bar itself, which is not correctly represented by the two considered numerical models. Similar results have been also obtained in [14], where it is underlined that the MC2010 bond-slip law tends to overestimate the tension stiffening contribution at the stabilized cracking stage. Furthermore, the introduction of the damage coefficient λ only slightly improves the numerical response.

As regards tension ties local behaviour, Figure 6 shows the comparisons in terms of force distribution in steel along the bar axis for different loading levels for STN12 sample. Similar results have been also obtained for sample STN16. In the experimental tests, 25 strain gauges were fixed onto the surface of the central part of the deformed bar at 25 mm centres, so to measure the variation of steel stresses as loading increases [14]. The steel force has been subsequently determined as $N_s = \varepsilon_s E_s A_s$. As can be seen from Fig. 6, both the 1D and 2D FE models are able to correctly capture the local effect of damage on bond caused by crack formation, even if some differences can be observed for bigger values of the applied load (P = 40 kN), since the experimental results highlight the presence of a sixth primary crack which has not been recognized in the experimental crack pattern scheme.

The distribution of tensile forces in concrete along the bar is shown for both STN12 and STN16 samples in Fig. 7, for a fixed value of the external load corresponding to the

formation of the last observed primary crack (respectively equal to P = 40 kN and P = 75 kN). Finally, Table 1 summarizes the calculated and experimental values of crack widths *w* at concrete surface in the stabilized cracking stage. As can be observed, both the two considered models provide a reasonable estimate of maximum crack openings, while the average value of crack width is generally overestimated.

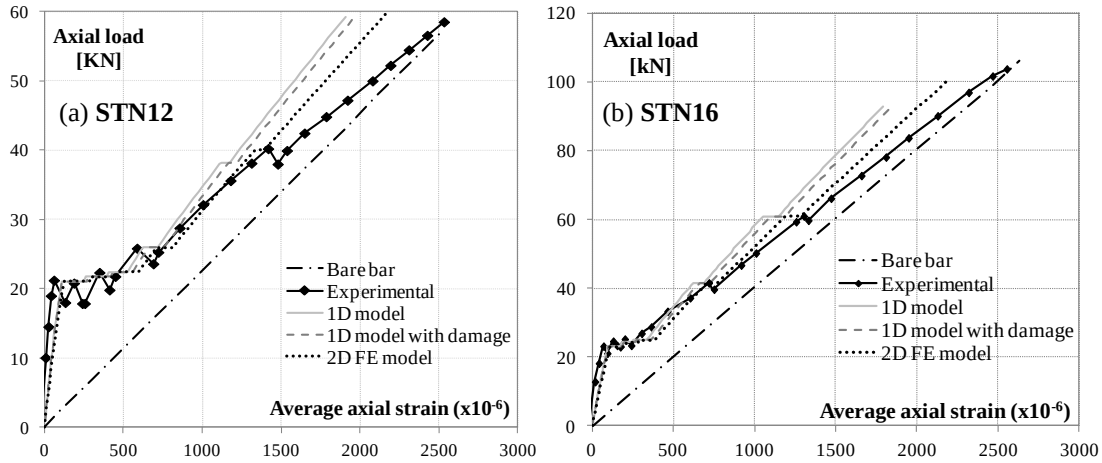

Figure 5. Comparisons between experimental [13] and numerical results for (a) STN12; (b) STN16 specimens, in terms of applied axial load-average axial strain.

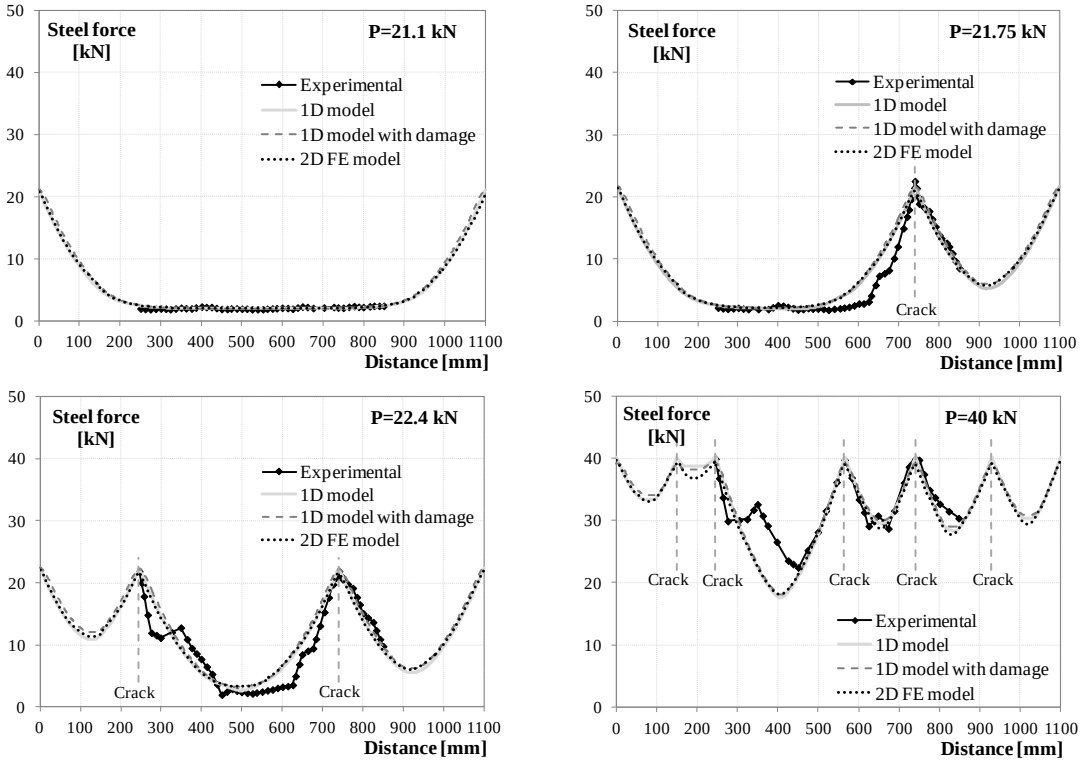

Figure 6. Comparisons between experimental [13,14] and numerical results for specimen STN12 in terms of steel force distribution along bar axis.

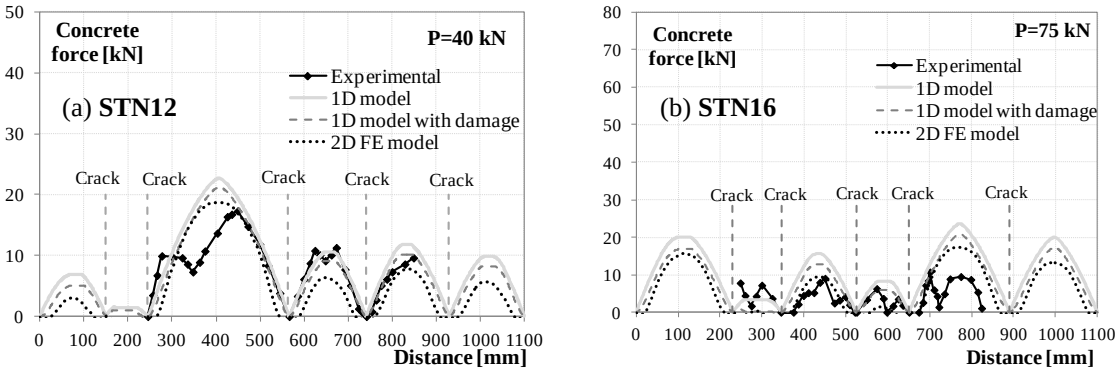

Figure 7. Comparisons between experimental [13,14] and numerical results for (a) STN12; (b) STN16 specimens, in terms of concrete force distribution along bar.

Table 1. Measured and calculated crack widths in the stabilized cracking stage.

	STN12			**STN16**		
	P [kN]	w_{avg} [mm]	w_{max} [mm]	P [kN]	w_{avg} [mm]	w_{max} [mm]
Exp. [13]	40	0.185	0.300	75	0.215	0.325
1D model	40	0.249	0.309	75	0.272	0.332
1D damage	40	0.258	0.331	75	0.282	0.347
2D model	40	0.243	0.318	75	0.269	0.332

CONCLUSIONS

As shown from the comparisons between numerical and experimental results, the proposed 1D model is able to correctly describe the local and global behaviour of axially loaded members, despite its intrinsic limitations, mainly related to its simplified hypotheses and limited computational efforts. For the considered case studies, the 1D model provides indeed the same response as 2D FE analyses, in which the diffusion of stresses is explicitly taken into account. As a consequence, it can be argued that the local behaviour of the investigated elements - and consequently the estimate of crack width, which is of primary importance at SLS - is mainly related to bond, which has been included in both numerical models. Anyway, a better prediction of the involved variables could be obtained through a proper improvement of the adopted bond-slip law, so to better include the effects of concrete damage due to primary cracking, as well as bond deterioration under increasing steel stresses. Further developments of this work will primarily concern these aspects and a more extensive validation of the proposed 1D model with more experimental tests, so to make it suitable for performing an extensive parametric study. The latter could be a powerful tool for investigating the relationship between crack width and bond parameters, like bar diameter, independently of the dispersion of material properties, which is unavoidable in experimental tests.

APPENDIX A

Considering matrix **A** (Eq. 2), all the terms are nil except the following ones:

$A_{1,3} = K_s \quad A_{1,4} = -K_s \quad A_{2,3} = -K_s \quad A_{2,4} = K_s \quad A_{3,1} = 1/(E_s A_s) \quad A_{4,2} = 1/(E_c A_c)$

where $K_s = n_b \, \pi \, \phi \, k_s$.

For the boundary conditions, in case of load control the non-zero terms of $\mathbf{B}_a$, $\mathbf{B}_b$ and **a** (Eq. 3) are:

$B_{a2,2} = 1 \quad B_{a3,3} = 1 \quad B_{a4,2} = 1 \quad B_{b1,1} = 1 \quad B_{b4,2} = -1 \quad a_1 = P$,

whereas, in case of displacement control, they become:

$B_{a2,2} = 1 \quad B_{a3,3} = 1 \quad B_{a4,2} = 1 \quad B_{b1,3} = 1 \quad B_{b4,2} = -1 \quad a_1 = \Delta L$.

At crack formation, the terms of $\mathbf{B}_c$, $\mathbf{B}_d$ and **b** are:

$B_{c1,1} = 1 \qquad B_{c1,2} = 1 \quad B_{c2,2} = 1 \quad B_{c3,2} = 1 \quad B_{c4,3} = 1$

$B_{d1,1} = -1 \qquad B_{d1,2} = -1 \quad B_{d3,2} = -1 \quad B_{d4,3} = -1$

$b_2 = \sigma_{ct} A_c$

REFERENCES

1. Borosnyói, A., Balázs, G.L. (2005) *Struct. Concr.* **6** (2), 53-62.
2. Gerstle, W., Ingraffea, A.R. (1991) *Concr. Int.*, **13** (1), 44-48.
3. Beeby, A.W. (1972) *Cement Concr. Ass.*, Techn. Rep. 42.468
4. Goto, Y. (1972) *J. American Concr. Inst.*, **68** (4), 244-51.
5. Beeby, A.W. (2004) *Struct. Concr.*, **5** (2), 71-83.
6. Beeby, A.W. et al. (2005) *Struct. Concr.*, **6** (4), 155-165.
7. Fantilli, A.P., Mihashi, H., Vallini, P. (2007) *Mater. Struct.*, **40**, 1099-1114.
8. Fantilli, A.P., Ferretti, D., Iori, I., Vallini, P. (1999) *European Structural Integrity Society (ESIS)*, **24**, 99-125
9. Ferretti, D., Savoia, M. (2003) *Eng. Frac. Mech.* **70**(7–8), 1069-1083.
10. Hordijk, D.A. (1992). In: *HERON*, **37** (1), pp. 1-77
11. CEB-FIP Bulletin No.65 (2012), Model Code 2010, Final draft - Vol 1.
12. Ascher, U.M., Mattheij, R.M.M., Russel, R.D. (1988) *Numerical solution of boundary value problems for ordinary differential equations*, Englewood Cliffs, NJ: Prentice Hall.
13. Wu, H.Q., Gilbert, R.I. (2008) *An experimental study of tension stiffening in reinforced concrete members under short-term and long-term loads*, UNICIV Report No R-449, The University of New South Wales, Sydney.
14. Wu, H.Q., Gilbert, R.I. (2009) *Eng. Struct.* **31**, 2380-2391.
15. Abaqus 6.10 (2010) *Online documentation*, Dassault Systémes Simulia Corp.